Acta Polytechnica **64**(4):368–378, 2024
https://doi.org/10.14311/AP.2024.64.0368
© 2024 The Author(s). Licensed under a CC-BY 4.0 licence
Published by the Czech Technical University in Prague

EFFECT OF SURFACE AREA ON THE WEAR PROPERTIES OF AL-BASED AUTOMOTIVE ALLOY AND THE ROLE OF SI AT EUTECTIC LEVEL

Mohammad Salim Kaiser[a,*], Al-Kabir Hossain[b]

[a] *International University of Business Agriculture and Technology, Innovation Centre, Dhaka-1230, Bangladesh*
[b] *Bangladesh University of Engineering and Technology, Department of Mechanical Engineering, Dhaka-1000, Bangladesh*
[*] corresponding author: dkaiser.res@iubat.edu

Abstract. The efficiency of an engine material is closely correlated with its surface area. In order to investigate wear properties, effect of surface contact area as well as silicon addition at the eutectic level of Al-Cu-Mg alloy has been studied. This test is performed under room atmosphere and dry sliding conditions using a standard pin-on-disk apparatus. Weight reduction method is adopted to measure the wear rate in microns to get more accurate results. A load varying from of 5 to 50 N and a constant sliding speed of $0.77\,\mathrm{m\,s^{-1}}$ are maintained throughout the test. The test results show that a lower contact surface area has a negative impact on the wear properties having higher wear rate, while the coefficient of friction of the alloy and Si addition into the alloy improve the properties to some extent. Reduction of the contact surface area increases the unit pressure and decreased material volume causes softening of the alloy matrix, resulting in a higher wear rate and coefficient of friction. The Si addition offers such an improvement mostly for an increase in strength via the Si-rich intermetallic formation. A microstructural study confirms a lower abrasive wear with a minor plastic deformation on the worn surfaces of Si added alloy and wear with higher contact surface. The Si-added alloys contain the fine and strong Si-rich intermetallic, which are responsible for such a smooth worn surface.

Keywords: Al-alloy, contract area, wear, friction, worn surfaces, micrographs.

1. Introduction

Cast Al-Si-Cu-Mg alloy is one of the most widely used materials in the automobile industry for manufacturing cylinder heads, engine blocks, pistons, bearings etc. [1, 2]. Among the different high-quality properties like wear and corrosion resistance, machinability, castability and the mechanical properties, the major considerable factor is wear and frictional behaviour of the alloy. So, in addition to the above, it is also suitable for complex shape castings in machine manufacturing and other sectors such as aviation, transportation, and construction [3–5]. In these materials, the alloying elements Cu and Mg are mostly considered because they provide age hardening properties during heat treatment. Supplementary elements like Ni, Fe, Sn, Cr, Zr, Ti, Sc, Er etc. are also added into these types of alloys for solute strengthening and grain refinement. It is not only considered for improving the alloy strength, but also serves different purposes [6–9]. The concentration of the chemical elements may also vary to achieve the desired purpose. For the best performance, Cu and Mg content usually varies from 1 to 4 wt. % and 0.5 to 1 wt. %, respectively [10, 11]. In terms of Si addition, the eutectic composition around 12.6 wt. % is the most favourable composition considering the overall properties. If the concentration of Si is lower or higher, the alloys are considered hypo-eutectic and hyper-eutectic, respectively [12–14].

Wear involves the removal of material through contact surface damage and deformation in subject to relative motion. Sliding speed, load, and the operating environment have a great impact on the wear rate and frictional performance of the alloys. Material properties, such as density, hardness, tensile strength etc., associated with the composition of the material also play an important role. Apart from these, wear resistance depends on a number of parameters, such as material shape, size, roughness, porosity, etc. More specifically, wear resistance can be increased by hardness and density of the material [15]. It was found that wear increases significantly with increasing load and sliding speed because of the frictional heat produced at the contact surface, which weakens the materials [16]. Previous research regarding the sliding environment has been used to investigate the wear and tribology properties. It has been observed that, in comparison to dry sliding conditions, wear rate and frictional coefficient decrease with the use of lubricants. It happens as a result of a thin film forming between the contact surfaces, which inhibits heat generation to keep the contact materials from softening and to reduce roughness. Similar observations have also been made about wear in corrosive environments [12, 17]. Due to its combined effect on subsurface cracking and the actual area of contact, porosity in the materials causes a progressive increase in wear rate in dry sliding conditions. However, in wet

sliding conditions, pores serve as lubricant reservoirs, which offers a significant advantage in terms of wear properties [18]. The friction and wear are constantly dependent on the characteristics of the two sliding surfaces and the wear properties decreases with a higher surface roughness [19, 20]. Thus, for a longer engine life, alloys with higher wear properties are required. Consequently, it is still now of a great importance to study the wear characteristics of these alloys under different conditions.

Nevertheless, there have not been sufficient studies on the wear behaviour of Al-based automotive alloys where the effect of contact surface area has been considered. The aim of this study is to assess the effect of Si at the eutectic level on the wear characteristics as the contact surfaces of the alloy are reduced. To complement the wear mechanism study, microstructural and fracture behaviour were also considered for both no and Si-added alloys.

2. Materials and methods

Al-Cu-Mg alloys with Si content at the eutectic level were prepared by conventional casting using pure aluminium, copper, magnesium, and the master alloy of Al–50%Si. A pit type natural gas furnace with a graphite crucible was used for melting the alloy at around 750 °C. Then it was stirred in order to homogenise the alloy at 700 °C, followed by pouring in mild steel mould of 20 mm × 200 mm × 300 mm preheated at 250 °C. Homogenous annealing was performed at 450 °C for 12 hours, solution treatment at 535 °C for 2 hours in an electrical resistance furnace, and then the alloys were rapidly quenched in cold salt bath. The chemical composition of the alloys, as analysed by spectrochemical methods, is shown in Table 1.

Two sets of specimens were considered for the wear study. The wear specimens, 12 mm in length and 5 mm in diameter, were machined from the two test alloys. To reduce the contact surface area, a 3 mm hole was drilled 5 mm deep into the specimens for a further set. In this study, the solid specimens of Alloy 1 were referred to as Alloy 1(S) and the drilled specimens as Alloy 1(H). Similarly, for Alloy 2, the solid specimens were referred to as Alloy 2(S) and the drilled specimens were referred to as Alloy 2(H). Artificial aging was performed for all the specimens at 200 °C for 240 minutes to achieve the peak strength as investigated earlier [21, 22]. The density of alloys was determined from their chemical composition. Hardness testing of the aged specimens was carried out using a Chinese-made SRS-150 Digital Rockwell Hardness Tester at B scale. About nine indentations were completed at different places on each polished surface of the aged specimens. The density of each alloy was calculated from the volume and weight measurements. At least five pieces of each sample were considered. The test of the tensile properties at room temperature was carried out according to ASTM E8 specification using Hydraulic Universal Testing Machine (Shimadzu, Japan, Model: UH-F1000 kN X). The sample gauge length was 25 mm and the strain rate was 10-3s-1. Seven tests were carried out for each condition. The surface roughness of the stainless steel disc was measured with Tylor-Hubson surface roughness tester, made in England. The roughness was measured seven times at different points and the average value was taken. XRD analyses of the cold-rolled alloys, aged for one hour at 100 °C, were carried out using a PANalytical Empyrean X-ray diffractometer (England made) with the Cu-Kα radiation and at a scanning rate of 1° min^{-1} and a Bragg angle 2θ ranging from 25° to 85°.

	Si	Cu	Mg	Fe	Ni	Al
Alloy 1	0.244	2.158	0.767	0.211	0.199	Balance
Alloy 2	12.656	2.130	0.770	0.311	0.277	Balance

Table 1. Chemical composition by wt. % of the two alloys.

The wear and frictional behaviour of both the alloys were observed in a pin-on-disc wear apparatus via G99-05 ASTM standard [23]. The capacity of the wear testing apparatus was 1hp and it was made in Bangladesh. The 309s stainless steel disc was considered for the counter surface material, whose average experimental hardness and roughness were HRB 95 and 0.45 µm, respectively. A load of 20 N was used for both specimens in the dry sliding condition, with the calculated contact pressures set at 1.02 MPa for the solid specimens and 1.59 MPa for ther hollow specimens. For this type of material, previous research considered the applied load to be roughly 20N. In other experiments, a load of 5 to 50 N was used [24, 25]. During the test, the disc rotated at 300 rpm on a 49 mm diameter track. Hence the calculated sliding speed was 0.77 m s^{-1} and variable distances from 231 m to 2 772 m were considered. All tests were performed under ambient conditions at 20 °C and 75 % humidity. At least nine readings were completed for every test of the material. The exact weight loss (ΔW), sliding distance (S.D.) and applied load (L) to the samples were considered to calculate the wear rate. The calculated sliding distances were obtained from the diameter of the track and the rotation of the disc. The friction coefficient (μ) was also determined from normalising the load cell (F) by the applied normal load (L). The following equations were applied to find the weight loss, specific wear rate (S.W.R.) and the friction coefficient:

$$\Delta W = W_{\text{initial}} - W_{\text{final}}, \tag{1}$$

$$\text{S.W.R.} = \frac{\Delta W}{\text{S.D.} \times L}, \tag{2}$$

$$\mu = \frac{F}{L}. \tag{3}$$

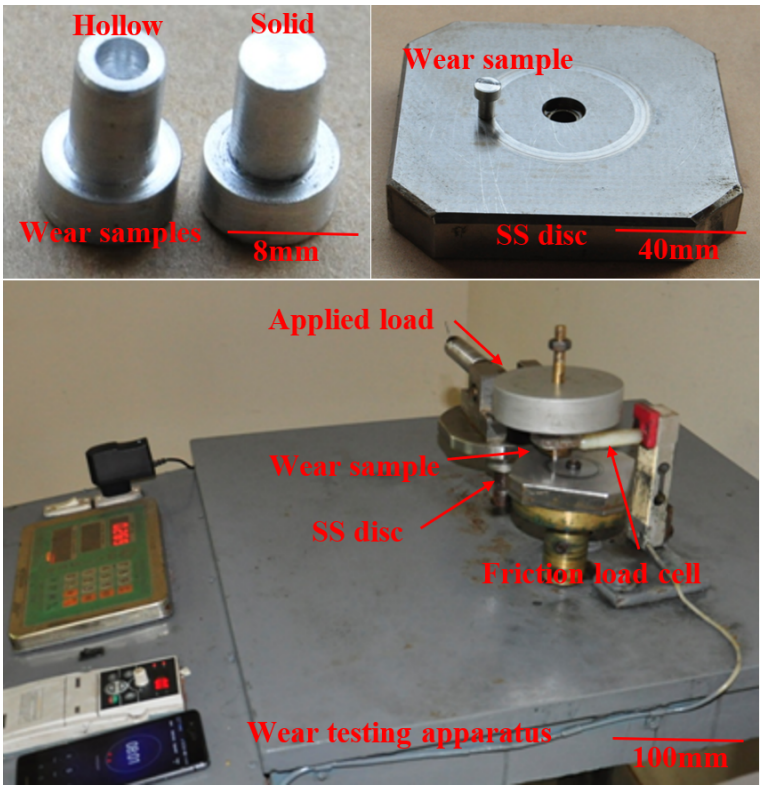

Figure 1. Photographs of specimens, stainless steel counter disc, and the testing apparatus of wear characteristics.

	Density [gm cm^{-3}]	Hardness [HRB]	UTS [MPa]	% elongation
Alloy 1	2.851 ± 0.007	63.7 ± 2	139 ± 10	5.4 ± 0.29
Alloy 2	2.812 ± 0.009	81 ± 3.1	245 ± 14	4.6 ± 0.26

Table 2. Physical and mechanical properties of the two test alloys.

Microstructural observations were performed by a Versamet-II-Microscope, where the specimens were polished with alumina and chemically etched with Keller's reagent through conventional metallographic techniques. The SEM analyses of the worn surface along with the fracture surface were conducted with the JEOL scanning electron microscope, JSM-5200. Four specimens at a time were attached to the top of the flat plate using double-sided carbon tape and the plate was seated in the specimen holder and fastened with a set of screws. Photographs of the specimens, the stainless steel counter disc, and the test setup are shown in Figure 1.

3. Results and discussion

3.1. Physical and mechanical properties

To give an idea of the physical and mechanical properties of both alloys, density, hardness, tensile strength, and elongation at break are tabulated in Table 2. Following the table, it confirms that density decreases by addition of Si into the alloy. The density of Si and Al is 2.329 gm cm^{-3} and 2.700 gm cm^{-3}, respectively, so the density of Si is lower than that of Al. The percentages of the other elements in the base Alloy 1 and Si-added Alloy 2 is similar apart from Si and Al. Thus, around 12.7 % Si addition makes the alloy lighter [26]. In addition, it has an opposite nature with higher hardness than the values of the base Alloy 1. During the ageing treatment, different types of intermetallic phases, such as Al_2Cu, Al_2CuMg, Mg_2Si, $Al_5Cu_2Mg_7Si_7$, and Al_5FeSi, are formed and these are responsible for the better hardness. Alloy 2 produces higher level of Si-rich intermetallic phases due to the the higher Si concentration in the alloy, resulting in higher hardness [21, 27].

It can be observed from the table that the Si added Alloy 2 is shows a higher tensile strength and Rockwell hardness. It was discussed earlier that ageing treatment forms different intermetallic phases in the alloy matrix, but phases Al_2Cu and Mg_2Si are responsible for increasing the tensile strength. Alloy 2 achieves the best strength through the additional Mg_2Si precipitates formed by the Si addition into the alloy [28]. The table also confirms that the percentage of elongation is reduced when the Si is added into the alloy. Addition of Si into the alloy means a higher fraction of Si-rich precipitates into the alloy matrix. These hinder the dislocation movement and make the alloys brittle, resulting in a lower elongation [29].

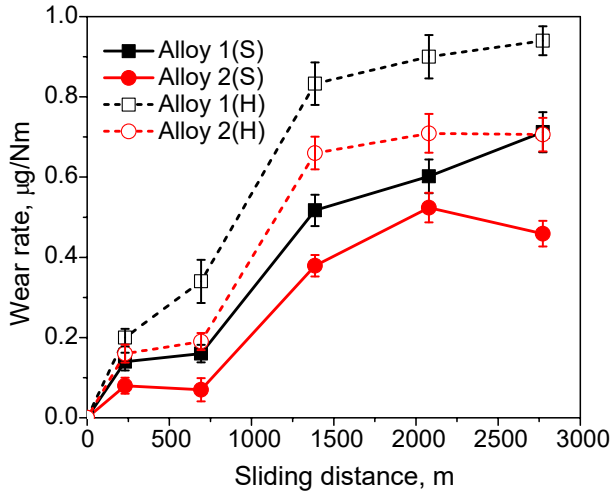

FIGURE 2. Discrepancy in wear rate by way of sliding distance of the solid and drilled specimens for both alloys.

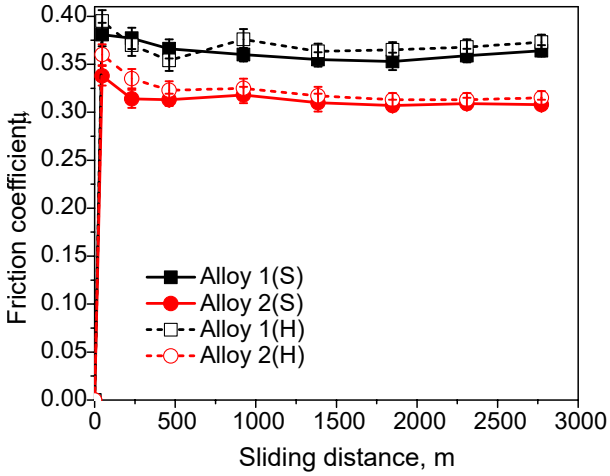

FIGURE 3. Discrepancy in coefficient of friction by way of sliding distance of the solid and drilled specimens for both alloys.

3.2. WEAR BEHAVIOUR

Based on the experimental results, the wear and fractional behaviour of the solid and hollow samples for both the alloys is plotted in the following Figures 2, 3 and 4. In the graphs, solid and drilled specimens of Alloy 1 are referred to as Alloy 1(S) and Alloy 1(H), respectively. Similarly, Alloy 2(S) and Alloy 2(H) are for Alloy 2. Sliding velocity of approximately 0.77 m s^{-1} is considered for all cases. The first is the wear rate versus sliding distance under a constant pressure of 20 N, which is 1.02 MPa for the solid specimen and 1.59 MPa for the drilled specimen, as shown in Figure 2. It can clearly be seen that as the sliding distance increases, the wear rate also increases for both alloys. The wear rate is higher for both the solid and drilled specimens of Alloy 1 than that of Si-added Alloy 2. Again, the wear intensity of the drilled specimens is higher than that of the solid specimens. The increasing phenomenon of wear rate is associated with softening of materials. Prolonged contact between the two mating surfaces generates heat through pressure and friction, causing the alloy material to soften. Thus, the weak alloy matrix makes it susceptible to damage [30]. This softness is high for the drilled specimens due to their relatively higher stress concentration at the contact surfaces. The drilled specimens consist of less contact area in addition to the volume of material, but the applied load is constant for all the specimens.

These well studied alloys are generally made up of the main element Al and various other alloying elements, such as Si, Cu, Mg, Ni, Fe etc. During heat treatment such as solution treatment followed by ageing, different intermetallic phases are formed, namely Al_2Cu, Al_2CuMg, Mg_2Si, $Al_5Cu_2Mg_7Si_7$, Al_3Ni, Al_3CuNi, Al_5FeSi, etc., into the Al matrix [10, 31]. Especially the formation of nano-sized Al_2Cu and Mg_2Si precipitate phases improve the wear and friction properties of the alloys. According to Archard's theory, the wear rate of harder alloys is always lower under dry sliding conditions [32]. These hard particles in the matrix have a higher load-carrying capacity, therefore improving the adhesion resistance of the alloys. In case of base Alloy 1, an insignificant amount Si-rich intermetallic phases is formed because of its impurity and the minor amount of Si. Alloy 2 forms a higher amount of Mg_2Si phase, which refines the grain structure and not only contribute to mechanical properties, but also improve the wear behaviour of the alloy. Sometimes, the presence of Mg in the alloy forms Al_3Mg_2 intermetallic phase, which initiates stress corrosion cracking and has a negative effect on the wear [33]. This is reduced by the formation of Mg_2Si, when the addition of Si creates bonds with Mg. The wear morphology also depends on the degree of oxidation formed during sliding [34]. The stable and hard oxide layer separates the contact surfaces, resulting in a lower wear rate. When the surface of the alloy is exposed to air, Mg_2Si forms more MgO and SiO_2 layers [35]. In addition, the fine and uniformly distributed Si phase generally increases the passivation at the edge during friction. As a result, the stress concentration on the matrix is reduced. The obtained results are supported by the physical and mechanical properties presented in Table 2.

Figure 3 provides information on the effects of frictional force at different sliding distances for both solid and hollow samples of base Alloy 1 and Si-added Alloy 2. It can clearly be seen that the coefficient of friction of the two specimens for the two alloys fluctuates in the early stages of sliding distances and then the decreasing nature is followed by the steady state. As the contacting surfaces are comparatively rougher at the beginning, the coefficient of friction is not constant at the beginning. The increase in the coefficient of friction can be attributed to the local adhesion of wear debris on the Al surface, as reported by earlier investigator [17]. Increasing the sliding distance increases the contact surface temperature, resulting in

higher oxidation of the surface. So, the coefficient of friction decreases slightly as it reduces direct metal contact [36, 37]. However, the coefficient of friction is relatively lower for Si-added Alloy 2 than that of base Alloy 1. The decreased frictional force can be attributed to better hardness and strength, as the low plastic deformation of the alloy at real contact areas can lead to decrease of coefficient of friction [38]. The drilled specimens always show higher coefficient of friction than solid ones, as expected, due to higher stress concentration with higher plastic deformation in real contact.

Figure 4 shows the discrepancy in average coefficient of friction for both solid and drilled specimens of the two tested alloys under different loads during dry sliding conditions. From this figure, it can clearly be seen that coefficient of friction decreases when the load increases. However, the nature and intensity of the trend is different for solid and drilled specimens. These phenomena in the coefficient of friction can be classified with the development of oxide layers on the mating surfaces of the alloys. When the load is increased, there is, as expected, an increase in temperature between the disc and pin surface which acts as a driving force for oxidation. Hence, higher load means lower coefficient of friction due to higher oxide formation [39]. Stable oxide layer reduces alloy surface to disc surface contact, reducing the coefficient of friction. In the case of the Si-added alloy, the Si particles are deformed into tiny fragments and act as a solid lubricant at the interface. These deformed particles carry the majority of the applied load under incessant sliding, so there is an inferior coefficient of friction. The rate of decrease is lower for the drilled specimens due to less oxidation caused by the lower contact area.

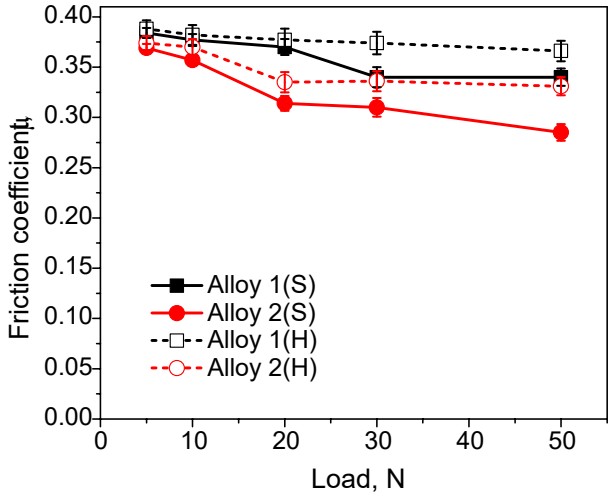

Figure 4. Discrepancy in coefficient of friction by way of applied load of the solid and drilled specimens for both alloys.

3.3. Optical microscopy

The worn surfaces by the optical microscopy of both solid and hollow specimens of the two alloys before and after 2 772 m of wear are shown in Figure 5. A sliding velocity of 0.77 m s^{-1} and a pressure of 20 N are used, which is 1.02 MPa for the solid specimen and 1.59 MPa for the drilled.

Both alloys exhibit smooth surfaces prior to wear and no signs of plastic deformation. Some spots are observed on the surface due to polishing with emery paper. Without etching, such microstructures do not provide any information. However, it consists of α-Al phase surrounded by different eutectic mixtures in the interdendritic matrix. Hence, the polished surfaces exhibit somewhat dissimilar tones since various alloying elements of different levels exist within the alloys. The tone is lighter or darker depending on the existing elements contained in the alloy. However, the lighter tone on the surface of the alloy containing 12.7Si became more prominent due to the increasing percentage of Si in the Al matrix [40]. Drilled specimens consist of a circular mark which is the abidance of the drill.

As can be seen from the photographs, the surfaces of the alloys become plastically deformed after wear and change in size and shape. Some grooves are observed parallel to the sliding direction by local flow of the surface material and subsequent detachment of material and surface cracks. This issue is more prominent for Alloy 1. It is because of the lower strength and higher elongation properties of Alloy 1 than those of Alloy 2 as shown in Table 2. These deformation behaviours are more pronounced for drilled specimens than for solid specimens, as hollow specimens carry higher stresses. Also, surface cracks are relatively smooth for the alloy containing Si, often from hard and fine Si-rich precipitates. Consequently, both the wear and friction are low for Si-added alloy.

Figure 6 shows the chemically etched microstructure of the two experimental alloys after the solution treatment followed by ageing at 200 °C for 240 minutes and further analysis using the worn surfaces shown in Figure 5. The microstructure of the base Alloy 1 is mainly composed of α-Al phase with various intermetallic particles distributed in intragranular and grain boundaries, there are no Si particles in the microstructure (Figure 6a). This type and the amount of second phases have a significant influence on the properties of the alloy. When Si is added at the eutectic level, Alloy 2 microstructure then consists of α-Al, eutectic Si, Si-rich and various other intermetallic particles (Figure 6b). The eutectic Si is distributed in the α-Al region, some even penetrating the entire α-Al grain, increasing the segregation effect within the matrix structure. The variation of silicon also refines the structure and the eutectic compassion elongated needle-like eutectic Si is formed [21, 41].

3.4. XRD study

Figure 7 shows the XRD patterns of both alloys in the T6 heat-treated condition. Alloy 1, the base alloy, shows peaks of Al phase and Al_2Cu. When Si is added

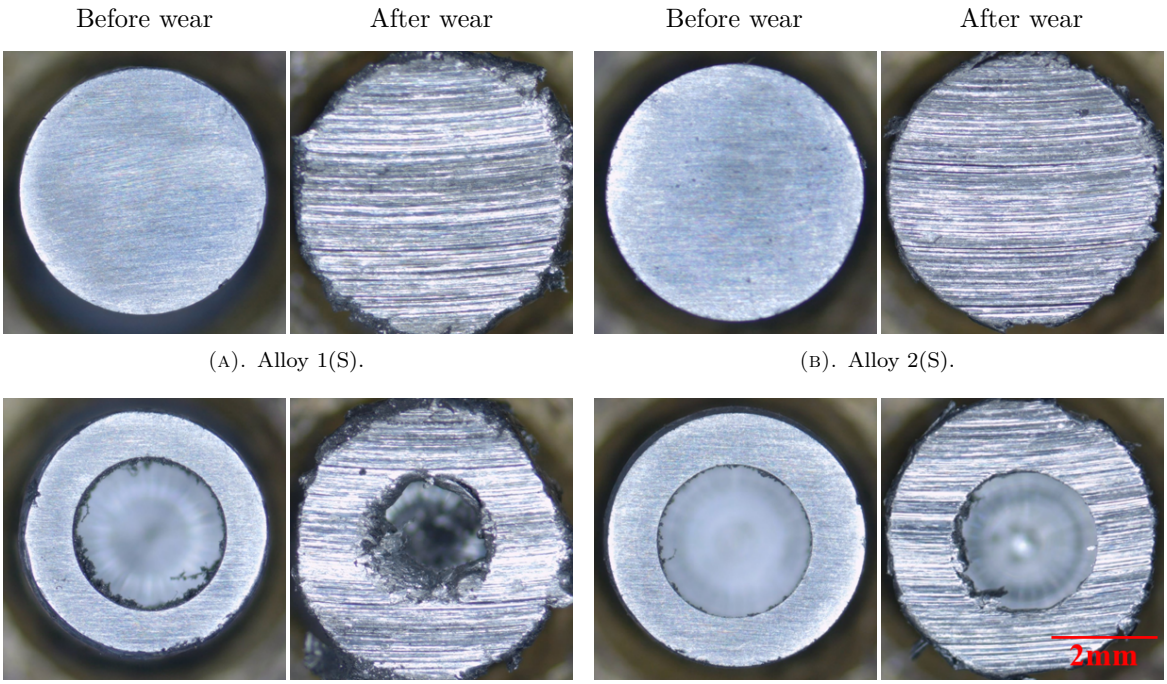

(A). Alloy 1(S). (B). Alloy 2(S).

(C). Alloy 1(H). (D). Alloy 2(H).

FIGURE 5. Surfaces images of the solid and drilled specimens for both alloys, polished before wear and after wear for a sliding distance of 2 772 m.

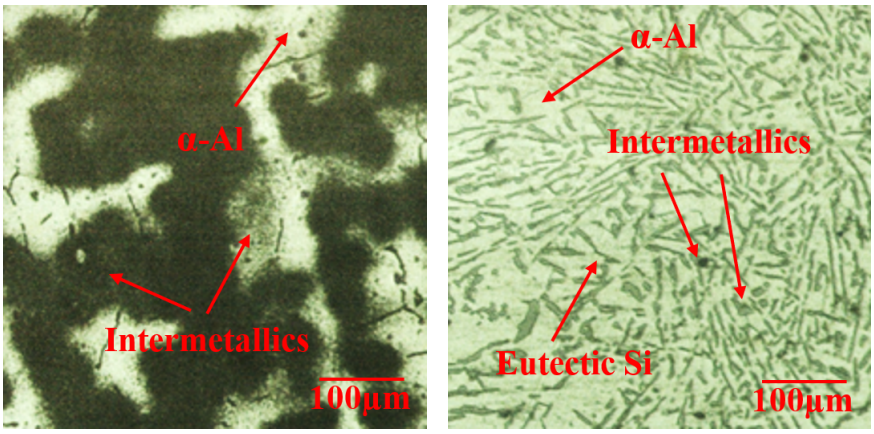

(A). Alloy 1. (B). Alloy 2.

FIGURE 6. Optical micrograph of Alloy 1 and Alloy 2 aged at 200 °C for 240 minutes corresponding to peak aged condition.

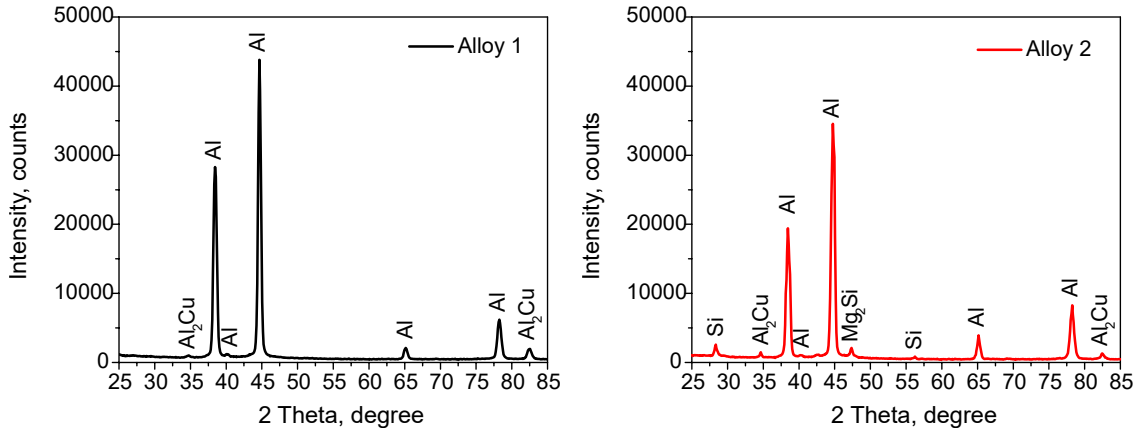

(A). Alloy 1. (B). Alloy 2.

FIGURE 7. XRD patterns of Alloy 1 and Alloy 2 aged at 200 °C for 240 minutes corresponding to peak aged condition.

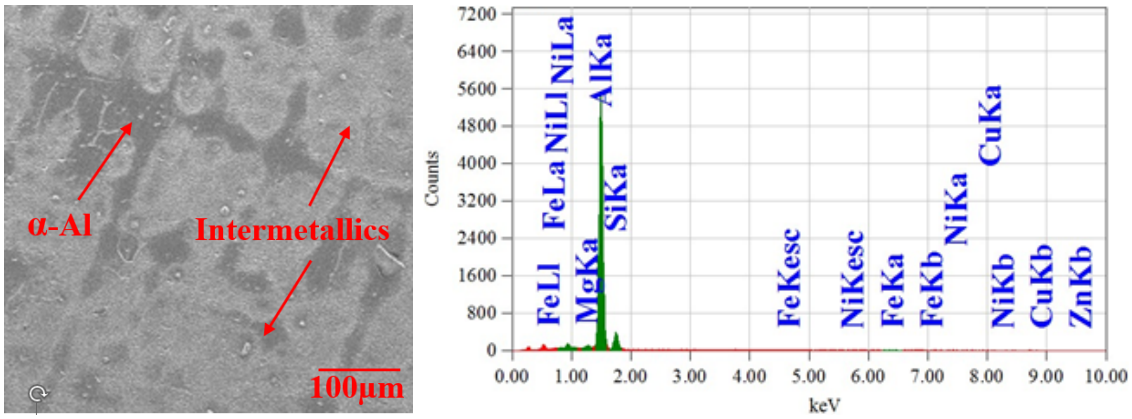

(A). Alloy 1.

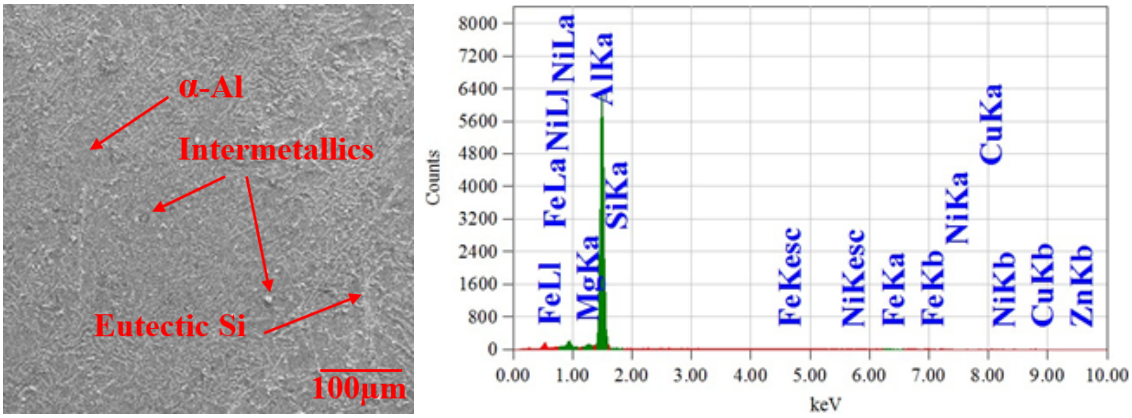

(B). Alloy 2.

Figure 8. SEM and EDX spectra of Alloy 1 and Alloy 2 aged at 200 °C for 240 minutes corresponding to peak aged condition.

to the base alloy, Alloy 2 produces two more peaks of Si and the silicon phase Mg_2Si. It can be seen that these two peaks result in a lower Al peak position level compared to Alloy 1. These two intermetallic phases, Al_2Cu and Mg_2Si, generally play an important role in strengthening of the discussed alloys. Other peaks are not clearly observed in the case of prior T6 heat treatment, because the corresponding intermetallics are in a very narrow range that is not detectable by this analysis [10, 42].

3.5. Scanning electron microscopy

The SEM with EDX spectra to match the optical images of the alloys are shown in Figure 8. Base Alloy 1 contains the α-Al phase with various intermetallic particles and traces of Si particles in the microstructure (Figure 8a) were detected. The corresponding EDX composition is 96.57 % Al, 0.17 % Si, 2.14 % Cu, 0.72 % Mg, and 0.40 % Ni in wt %. Similarly, Si-added Alloy 2 contains α-Al, needle-like eutectic Si, with or without Si-rich other intermetallics (Figure 8b). The EDX composition of Si-added Alloy 2 is 85.37 % Al, 11.43 % Si, 1.71 % Cu, 0.63 % Mg, 0.29 % Ni, 0.26 % Zn, and 0.32 % Fe.

Solid and drilled specimen surfaces of both the alloys are obtained by an electron scanning microscopy from the wear evaluation at a sliding velocity of 0.77 m s^{-1} and a sliding distance of 2 772 m. Their worn surfaces are shown in Figure 9 to investigate the mechanism of wear. It clearly indicates abrasive wear in the solid specimen of the base Alloy 1(S), exposing grooves due to the abrading action of the strong particles (Figure 9a). For the identical Si-added Alloy 2(S), the micrograph shows some small cracks, grooves, and delaminations, clearly indicating a mixture of abrasive and delaminating wear (Figure 9c). For the drilled specimens of the base Alloy 1(H), under the same wear setting, the micrograph showed deep grooves of abrasive wear (Figure 9b). In addition, the drilled specimens of Si-added Alloy 2(H) also showed cracks with narrow grooves of abrasive and delaminating wear too (Figure 9d). It was already stated that the samples are used in its peak aged condition. So, nano-sized Al_2Cu and nano-sized Mg_2Si phases, which enhance the wear resistance, precipitate in the matrix. In addition, formation of Mg_2Si phase also refines the grain structure of the alloy. That is why Alloy 2 has smooth surfaces. In case of the drilled specimens, relatively higher surface damage is observed due to greater unit pressure on the surface [21].

To complement the images of the worn surfaces, a further SEM of the experimental tensile fracture

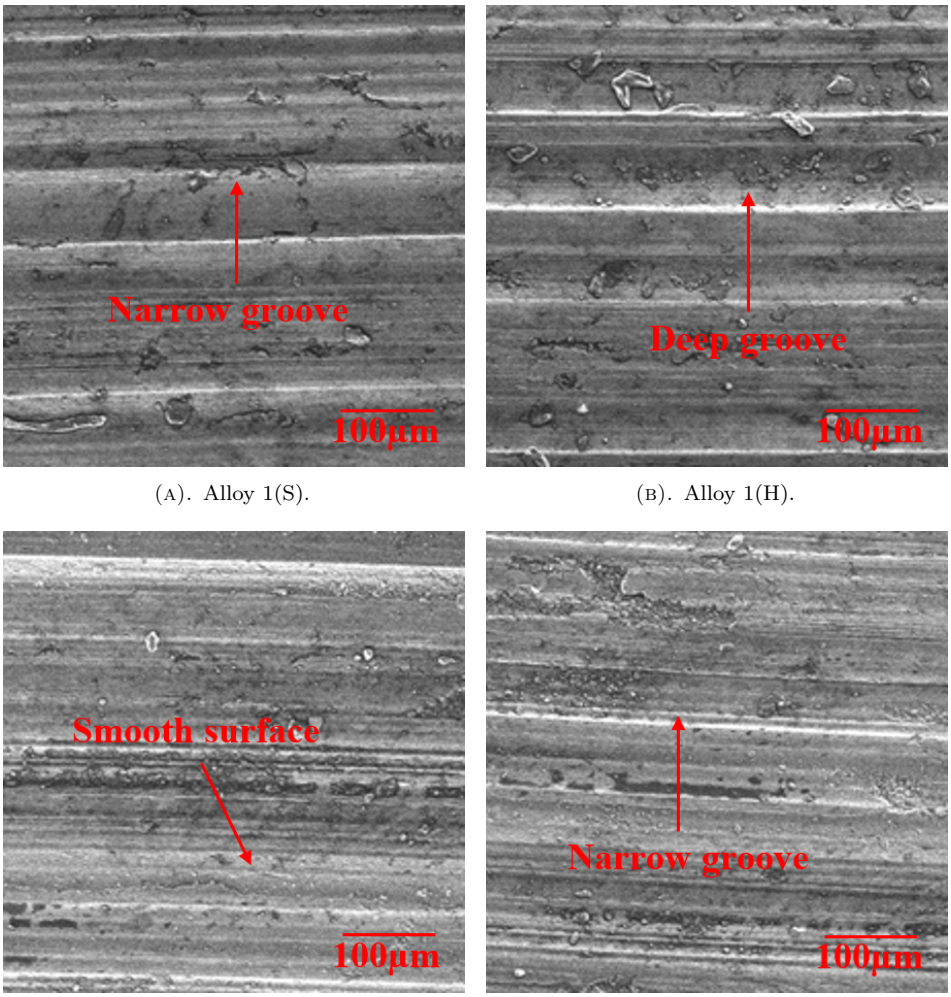

(A). Alloy 1(S). (B). Alloy 1(H).

(C). Alloy 2(S). (D). Alloy 2(H).

FIGURE 9. Worn surfaces after wear for 2 772 m of sliding distance under SEM.

surface morphology is also shown in Figure 10. A clear difference in fracture mode was observed between them. Where the base Alloy 1 shows the fracture throughout the grain boundary with a large number of voids in the matrix evenly distributed in the micrograph (Figure 10a and 10b). This is the most common mode of fracture, such as intergranular fracture with grain boundary. There are multiple dimple morphologies and ductile α-phase fractures indicative of composite fracture [43]. The figure also demonstrated that the plane of the fracture depends on the orientation of the grain. The Si-added Alloy 2 shows signs of additional crack propagation caused by the enormous cleavage of the niddle-type shapes and brittle Si rich intermetallics (Figure 10c and 10d). Given the fact that the Si content increased, a large amount of these intermetallics would expected in the alloys, extending the cracks. The amount of crack direction also increases at fracture surfaces. Different types of intermetallic phases are observed in this type of alloy as it contains different levels of alloying elements, but plate-shaped intermetallics are the most detrimental to mechanical properties [44, 45]. Relatively deep fracture is observed for drilled specimens, such as Alloy 1(H) and Alloy 2(H), compared to the higher surface area of Alloy 1(S) and Alloy 2(S). It is obvious that it is caused by higher pressure due to higher thrust and temperature in the case of hollow samples. But the mode of fracture is identical for each alloy.

4. Conclusion

The wear characteristics of Al-based automotive alloys with Si addition under different surface contact areas have been evaluated and several conclusions can be drawn from the research results:

- The reduced surface area of contact provides a higher wear rate along with the coefficient of friction of the alloy. The reduction of contact surface area increases the unit pressure and the reduced material volume causes softening of the alloy matrix, resulting in a higher wear rate.
- Si decreases the softening tendency to some extent. The Si-added alloy achieved higher hardness due to a variety of rigid Si-rich intermetallic phases through the ageing treatment. Consequently, it improves the wear characteristics of the Al-based automotive alloys. The Si-added alloy has a lower

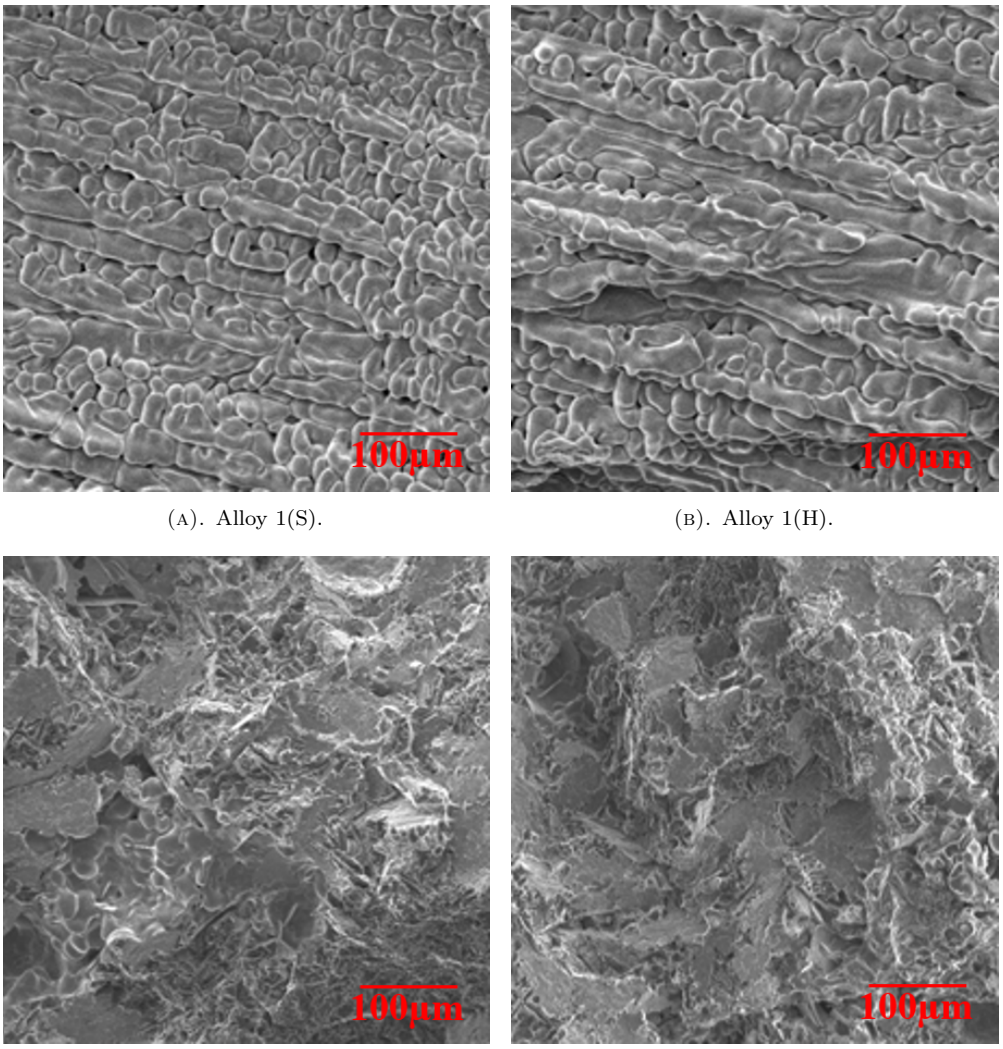

(a). Alloy 1(S). (b). Alloy 1(H).

(c). Alloy 2(S). (d). Alloy 2(H).

Figure 10. SEM of the experimental tensile fracture surface morphology.

coefficient of friction due to its higher hardness and the Si-rich particles act as a solid lubricant.

- The worn surfaces of Si-added alloy under dry sliding condition have a lower abrasive wear and plastic deformation due to grain the refining effect and Mg_2Si phase formation preventing the wear. These deformations are higher for the drilled specimens as they carry the higher stress.
- The surface roughness of the material is very important in terms of wear rate and coefficient of friction. The contact surface of drilled specimens is very small. Therefore, it could not be measured. For a better understanding, large area samples can be combined.

Acknowledgements

The corresponding author would like to express his gratitude to Prof. Selina Nargis, the Treasurer & Director Administration at IUBAT, for her valuable support and encouragement in promoting research activities at the university. Her efforts in promoting collaborations with other institutions are also commendable.

References

[1] P. Zhou, D. Wang, H. Nagaumi, et al. Microstructural evolution and mechanical properties of Al-Si-Mg-Cu cast alloys with different Cu contents. *Metals* **13**(1):98, 2023. https://doi.org/10.3390/met13010098

[2] M. Javidani, D. Larouche. Application of cast Al-Si alloys in internal combustion engine components. *International Materials Reviews* **59**(3):132–158, 2014. https://doi.org/10.1179/1743280413Y.0000000027

[3] H. Ye. An overview of the development of Al-Si-alloy based material for engine applications. *Journal of Materials Engineering and Performance* **12**(3):288–297, 2003. https://doi.org/10.1361/105994903770343132

[4] A. Mostafa, N. Alshabatat. Microstructural, mechanical and wear properties of Al-1.3%Si alloy as compared to hypo/hyper-eutectic compositions in Al-Si alloy system. *Crystals* **12**(5):719, 2022. https://doi.org/10.3390/cryst12050719

[5] M. S. Kaiser. Effects of solution treatment on wear behaviour of Al-12Si-1Mg piston alloy containing trace Zr. *MAYFEB Journal of Materials Science* **1**:27–38, 2016.

[6] Z. Yang, X. He, B. Li, et al. Influence of Si, Cu, B, and trace alloying elements on the conductivity of the Al-Si-Cu alloy. *Materials* **15**(2):426, 2022. https://doi.org/10.3390/ma15020426

[7] H. Zhang, B. Chen, J. Hao, et al. Effects of Cu/Er on tensile properties of cast Al-Si alloy at low temperature. *Materials* **16**(3):902, 2023. https://doi.org/10.3390/ma16030902

[8] M. N. Ervina Efzan, H. J. Kong, C. K. Kok. Review: Effect of alloying element on Al-Si alloys. In *Materials, Industrial, and Manufacturing Engineering Research Advances 1.1*, vol. 845 of *Advanced Materials Research*, pp. 355–359. Trans Tech Publications Ltd, 2014. https://doi.org/10.4028/www.scientific.net/AMR.845.355

[9] A. A. Khan, M. R. Shoummo, M. S. Kaiser. Surface quality of Fe, Ni and Cr added hyper-eutectic Al-Si automotive alloys under up-milling and down-milling operation. *Journal of Mechanical Engineering Science and Technology (JMEST)* **6**(1):9–22, 2022. https://doi.org/10.17977/um016v6i12022p009

[10] S.-S. Ahn, S. Pathan, J.-M. Koo, et al. Enhancement of the mechanical properties in Al-Si-Cu-Fe-Mg alloys with various processing parameters. *Materials* **11**(11):2150, 2018. https://doi.org/10.3390/ma11112150

[11] M. Zhang, Y. Tian, X. Zheng, et al. Research progress on multi-component alloying and heat treatment of high strength and toughness Al-Si-Cu-Mg cast aluminum alloys. *Materials* **16**(3):1065, 2023. https://doi.org/10.3390/ma16031065

[12] M. S. Kaiser, A. A. Khan. Role of silicon on the tribological performance of Al-based automotive alloys and the effect of used motor oil. *Tribologia – Finnish Journal of Tribology* **39**(3–4):12–20, 2022. https://doi.org/10.30678/fjt.120669

[13] N. Kang, P. Coddet, C. Chen, et al. Microstructure and wear behavior of *in-situ* hypereutectic Al-high Si alloys produced by selective laser melting. *Materials & Design* **99**:120–126, 2016. https://doi.org/10.1016/j.matdes.2016.03.053

[14] M. Al Nur, A. A. Khan, S. Dev Sharma, M. S. Kaiser. Electrochemical corrosion performance of Si-doped Al-based automotive alloy in 0.1 M NaCl solution: Original scientific paper. *Journal of Electrochemical Science and Engineering* **12**(3):565–576, 2022. https://doi.org/10.5599/jese.1373

[15] S. J. S. Chelladurai, S. S. Kumar, N. Venugopal, et al. A review on mechanical properties and wear behaviour of aluminium based metal matrix composites. In *Materials Today: Proceedings*, vol. 37, pp. 908–916. 2021. https://doi.org/10.1016/j.matpr.2020.06.053

[16] G. Li, S. Hao, W. Gao, Z. Lu. The effect of applied load and rotation speed on wear characteristics of Al-Cu-Li alloy. *Journal of Materials Engineering and Performance* **31**(7):5875–5885, 2022. https://doi.org/10.1007/s11665-022-06613-x

[17] G. E. Totten (ed.). *ASM handbook, Volume 18: Friction, lubrication and wear technology*. ASM International, Materials Park, USA, 1992.

[18] M. A. Islam, Z. N. Farhat. Effect of porosity on dry sliding wear of Al-Si alloys. *Tribology International* **44**(4):498–504, 2011. https://doi.org/10.1016/j.triboint.2010.12.007

[19] V. Romanova, R. Balokhonov, O. Zinovieva, et al. The relationship between mesoscale deformation-induced surface roughness, in-plane plastic strain and texture sharpness in an aluminum alloy. *Engineering Failure Analysis* **137**:106377, 2022. https://doi.org/10.1016/j.engfailanal.2022.106377

[20] I. V. Lytvynenko, P. O. Maruschak, S. A. Lupenko, P. V. Popovych. Modeling of the ordered surface topography of statically deformed aluminum alloy. *Materials Science* **52**(1):113–122, 2016. https://doi.org/10.1007/s11003-016-9933-1

[21] S. Toschi. Optimization of A354 Al-Si-Cu-Mg alloy heat treatment: Effect on microstructure, hardness, and tensile properties of peak aged and overaged alloy. *Metals* **8**(11):961, 2018. https://doi.org/10.3390/met8110961

[22] M. S. Kaiser, A. S. W. Kurny. Effect of scandium on the grain refining and ageing behaviour of cast Al-Si-Mg alloy. *Iranian Journal of Materials Science & Engineering* **8**(4):1–8, 2011.

[23] J. R. Davis (ed.). *Metals handbook desk edition, 2^{nd} edition*. ASM International, Ohio, USA, 1998. ISBN 978-0-87170-654-6.

[24] M. M. Khan, A. Dey, M. I. Hajam. Experimental investigation and optimization of dry sliding wear test parameters of aluminum based composites. *Silicon* **14**(8):4009–4026, 2022. https://doi.org/10.1007/s12633-021-01158-5

[25] A. Mostafa, N. Alshabatat. Microstructural, mechanical and wear properties of Al-1.3%Si alloy as compared to hypo/hyper-eutectic compositions in Al-Si alloy system. *Crystals* **12**(5):719, 2022. https://doi.org/10.3390/cryst12050719

[26] I. J. Polmear. *Light alloys: Metallurgy of the light metals*. Arnold, London, UK, 3rd edn., 1995.

[27] S. Nikzad Khangholi, M. Javidani, A. Maltais, X.-G. Chen. Investigation on electrical conductivity and hardness of 6xxx aluminum conductor alloys with different Si levels. In *MATEC Web of Conferences*, vol. 326, p. 08002. 2020. https://doi.org/10.1051/matecconf/202032608002

[28] A. K. Gupta, D. J. Lloyd, S. A. Court. Precipitation hardening in Al-Mg-Si alloys with and without excess Si. *Materials Science and Engineering: A* **316**(1–2):11–17, 2001. https://doi.org/10.1016/S0921-5093(01)01247-3

[29] F.-b. Meng, H.-j. Huang, X.-g. Yuan, et al. Effect of Si addition on microstructure and mechanical properties of Al-Mg-Si-Zn alloy. *China Foundry* **17**(1):15–20, 2020. https://doi.org/10.1007/s41230-020-9102-x

[30] M. S. Prabhudev, V. Auradi, K. Venkateswarlu, et al. Influence of Cu addition on dry sliding wear behaviour of A356 alloy. In *Procedia Engineering*, vol. 97, pp. 1361–1367. 2014. https://doi.org/10.1016/j.proeng.2014.12.417

[31] Y. Yang, K. Yu, Y. Li, et al. Evolution of nickel-rich phases in Al-Si-Cu-Ni-Mg piston alloys with different Cu additions. *Materials & Design* **33**:220–225, 2012. https://doi.org/10.1016/j.matdes.2011.06.058

[32] J. F. Archard. Contact and rubbing of flat surfaces. *Journal of Applied Physics* **24**(8):981–988, 1953. https://doi.org/10.1063/1.1721448

[33] M. S. Kaiser, M. A. Matin, K. M. Shorowordi. Role of magnesium and minor zirconium on the wear behavior of 5XXX series aluminum alloys under different environments. *Journal of Mechanical and Energy Engineering* **4**(3):209–220, 2020. https://doi.org/10.30464/jmee.2020.4.3.209

[34] H.-J. Kim, A. Emge, S. Karthikeyan, D. A. Rigney. Effects of tribooxidation on sliding behavior of aluminum. *Wear* **259**(1–6):501–505, 2005. https://doi.org/10.1016/j.wear.2005.01.043

[35] R. Escalera-Lozan, M. I. Pech-Canul, M. A. Pech-Canul, et al. The role of Mg_2Si in the corrosion behavior of Al-Si-Mg alloys for pressureless infiltration. *The Open Corrosion Journal* **3**:73–79, 2010. https://doi.org/10.2174/1876503301003010073

[36] K. N. D. Malleswararao, I. N. N. Kumar, B. Nagesh. Friction and wear properties of rapid solidified H-Al-17Si alloys processed by UV assisted stir – squeeze casting with DLC-star (CrN + a-c:H) coating under HFRR. *Tribology in Industry* **42**(4):529–546, 2020. https://doi.org/10.24874/ti.870.04.20.09

[37] S. M. Aouadi, H. Gao, A. Martini, et al. Lubricious oxide coatings for extreme temperature applications: A review. *Surface and Coatings Technology* **257**:266–277, 2014. https://doi.org/10.1016/j.surfcoat.2014.05.064

[38] A. J. W. Moore, W. J. McG. Tegart. Relation between friction and hardness. *Proceedings of the Royal Society of London Series A Mathematical and Physical Sciences* **212**(1111):452–458, 1952. https://doi.org/10.1098/rspa.1952.0234

[39] S. A. Kori, T. M. Chandrashekharaiah. Studies on the dry sliding wear behaviour of hypoeutectic and eutectic Al-Si alloys. *Wear* **263**(1–6):745–755, 2007. https://doi.org/10.1016/j.wear.2006.11.026

[40] M. S. Kaiser, M. R. Qadir, S. Dutta. Electrochemical corrosion performance of commercially used aluminium engine block and piston in 0.1 M NaCl. *Journal of Mechanical Engineering* **45**(1):48–52, 2015. https://doi.org/10.3329/jme.v45i1.24384

[41] X. Li, H. Yan, Z.-W. Wang, et al. Effect of heat treatment on the microstructure and mechanical properties of a composite made of Al-Si-Cu-Mg aluminum alloy reinforced with SiC particles. *Metals* **9**(11):1205, 2019. https://doi.org/10.3390/met9111205

[42] B. Sirahbizu Yigezu, M. Mahapatra, P. Jha. Influence of reinforcement type on microstructure, hardness, and tensile properties of an aluminum alloy metal matrix composite. *Journal of Minerals and Materials Characterization and Engineering* **1**(4):124–130, 2013. https://doi.org/10.4236/jmmce.2013.14022

[43] S. Lynch. A review of underlying reasons for intergranular cracking for a variety of failure modes and materials and examples of case histories. *Engineering Failure Analysis* **100**:329–350, 2019. https://doi.org/10.1016/j.engfailanal.2019.02.027

[44] R. Rashid, S. H. Masood, D. Ruan, et al. Effect of energy per layer on the anisotropy of selective laser melted AlSi12 aluminium alloy. *Additive Manufacturing* **22**:426–439, 2018. https://doi.org/10.1016/j.addma.2018.05.040

[45] D. A. Lados, D. Apelian, J. F. Major. Fatigue crack growth mechanisms at the microstructure scale in Al-Si-Mg cast alloys: Mechanisms in regions II and III. *Metallurgical and Materials Transactions A* **37**(8):2405–2418, 2006. https://doi.org/10.1007/BF02586215